Engineering Structures 31 (2009) 2436–2447

Contents lists available at ScienceDirect

Engineering Structures

journal homepage: www.elsevier.com/locate/engstruct

Edge debonding in FRP strengthened beams: Stress versus energy failure criteria

A. Carpinteri, P. Cornetti *, N. Pugno

Department of Structural Engineering and Geotechnics, Politecnico di Torino, Turin, Italy

ARTICLE INFO

Article history:
Received 23 October 2008
Received in revised form
6 April 2009
Accepted 25 May 2009
Available online 18 June 2009

Keywords:
FRP strips
Strengthening
Failure criteria
Fracture mechanics
Energy release rate
Equivalent beam model
Shear lag model

ABSTRACT

In the present paper we analyse the edge debonding failure of a beam strengthened by a fibre reinforced polymer. As well known from the literature, a stress concentration is found at the edge of the reinforcement which triggers the debonding of the fibre reinforced polymer strip when the load reaches a certain critical threshold. Two failure criteria are proposed to study the debonding mechanism. The former is a stress assessment criterion, i.e. failure takes place whenever the maximum shearing stress reaches a limit value (the interfacial bond strength). The latter is an energy, fracture mechanics criterion, i.e. failure takes place as the strain energy release rate reaches a critical value (the interfacial fracture energy). It is argued that the energy criterion is more effective to address the edge debonding failure mode. However, under the assumption of shear lag behaviour for the adhesive layer between the beam and the reinforcement, a general rule linking the two approaches is set, thus providing the key to bypass the rather complicated energetic analysis. The final part of the paper is devoted to the crack instabilities that may occur after the debonding initiates, i.e. snap–back and snap-through phenomena. The size effect is then investigated by means of a dimensional analysis and a simplified formula providing the critical load is proposed that could be useful in engineering practice.

1. Introduction

Structural rehabilitation is required whenever design mistakes, executive defects or unexpected loading conditions are assessed. Retrofitting techniques aim to increase the load carrying capacity of the structure, or to reduce its deformations. Among the different rehabilitation strategies, bonding of Fibre Reinforced Polymers (FRP) sheets is becoming more and more popular, especially for what concerns concrete structure [1] although applications to metallic structures are quite common too [2]. The advantages of this technique are several. FRP strips are easy to install and cause a minimum increase in dimension; furthermore, they have a high strength, a light weight and a long durability. The growing interest of the Scientific Community is testified by the recent publication of new guidelines and standards for the rehabilitation of reinforced concrete structures [3–5].

The structural behaviour of FRP-strengthened members is substantially different from that of the original un-reinforced structures and, even more important, new failure modes may occur. Among the various failure modes observed, a special interest has been recently devoted to the edge debonding of the FRP because of its brittle and catastrophic features, the propagation of the interfacial crack being highly unstable. It is worth noting that edge debonding of the reinforcement strip is a failure mechanism that may occur both in concrete as well as in metallic FRP-strengthened beams. On the other hand, concrete beams may fail because of an interfacial crack in its turn induced by a flexural crack inside the concrete member. This failure mechanism is named IC-debonding (i.e. intermediate crack induced debonding) and is characterised by an interfacial crack running toward the edge, i.e. in the opposite direction with respect to what happens in the edge debonding failure mechanisms. Although the model that is developed in the present paper could be extended to take the IC-debonding into account [6], only the edge debonding will be dealt with in what follows (see also [7]).

In order to predict the critical load at which the edge debonding phenomenon takes place, several models have been proposed to evaluate the interfacial stresses. They all focus onto the prediction of the stresses in the vicinity of the edge of the FRP strip. These stresses are then used to predict the critical load. An accurate review of these models can be found in the paper by Muckopadhyaya and Swamy [8], which ends with the conclusion that the existing models are too complex to be used in practical designs.

However, because of the brittleness of the debonding process, an energy approach seems to be more effective, since stress-based failure criteria are more suitable for gradual and ductile failures. An energy-based fracture criterion has recently been proposed by Rabinovitch [9] and, later, by Colombi [10], by applying the linear elastic fracture mechanics (LEFM) concept of strain energy release rate (SERR). In other words, the edge debonding process is assumed to begin when the energy release due to an infinitesimal crack

* Corresponding author. Tel.: +39 0115644901; fax: +39 0115644899.
E-mail address: pietro.cornetti@polito.it (P. Cornetti).

0141-0296/$ – see front matter © 2009 Elsevier Ltd. All rights reserved.
doi:10.1016/j.engstruct.2009.05.015

growth is equal or higher than a critical value, i.e. the interfacial fracture energy. The aforementioned papers show how simplified models assuming a constant stress field across the adhesive layer thickness can be used to predict the SERR. However, the energetic approach is much more complicated with respect to the strength-based approach and the SERR has to be evaluated numerically by comparing the energetic state of the whole structure before and after a small interfacial crack growth. This makes the LEFM failure criterion less attractive for engineering design purposes.

The present paper starts by reviewing two basic models often used to analyse reinforced beams: the equivalent beam model and the more refined shear lag model. While the former disregards any compliance of the adhesive layer connecting the structure with the reinforcement, the latter model assumes that the adhesive layer acts as a shear lag, i.e. only shear stresses constant over its thickness are considered. This is a quite common assumption in structural mechanics problems: its first application dates back to Volkersen [11]. For what concerns steel plate and FRP strengthened beams, models based on similar assumptions have been applied and developed by a number of researchers: see, e.g., Vilnay [12], Triantafillou and Deskovic [13], Taljsten [14], Malek et al. [15], Smith and Teng [16] and references herein. However, following the papers by Rabinovitch [9] and Colombi [10], the stress field provided by the shear lag model is here used to apply the energetic LEFM failure criterion. With respect to the cited papers, the novelty is that a relationship, holding for any shear lag model, between the SERR and the stress field is proven for the first time. It provides the key to bypass the complicated energetic approach, making use of the much more simple stress analysis. The energetic failure criterion can hence be expressed analytically. It is believed that this finding can be useful for including debonding failure assessment in practical design codes.

Finally we will focus the attention upon the post-peak structural behaviour. By obtaining analytically the load vs. deflection curve, we highlight the possible rising of snap–back and snap-through instabilities according to test control [17–20].

A similar approach, applied to analyse delamination in a different geometry, has been recently proposed by Andrews et al. [21]. Moreover, among recent works based on neighbouring arguments, we wish to cite: the paper by Greco et al. [22] for the evaluation of the strain energy release rate, the work by Carpinteri et al. [23] based on the elastic mismatch between concrete and FRP; the paper by Ferracuti et al. [24] on numerical approaches to FRP debonding.

2. Equivalent beam model

In his excellent paper [9], Rabinovitch, in order to address the problem of FRP-strengthened beams, considers four different models of increasing complexity: the classical equivalent beam model, the one parameter elastic foundation model, the two parameter elastic foundation model and the higher order model. In the first model the compliance of the adhesive layer between the beam and the reinforcement is disregarded. The second and the third models are sometimes referred to as spring models, since the adhesive layer is represented as a bed of, respectively, horizontal springs and horizontal and vertical springs. Finally, according to the higher order model, the adhesive is modelled as a fully bi-dimensional elastic medium. In every model, classical Euler–Bernoulli beam theory is used for the beam and the FRP plate.

In the present paper we restrict our analysis to the first two models. This choice allows us to express all the results in a closed, analytical form.

The easiest model to handle beams strengthened by FRP is the so-called equivalent beam (EB) model, based on the assumption of a planar cross section for the whole structure. Let us refer to a

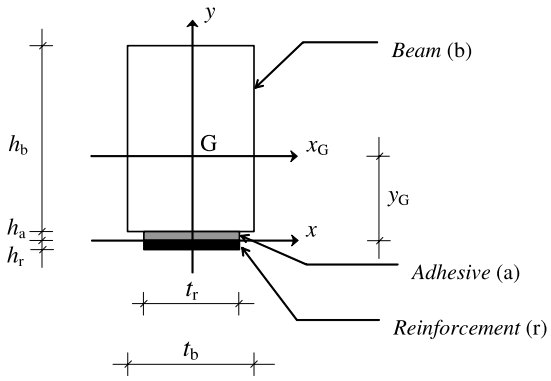

Fig. 1. Geometry of the reinforced cross section.

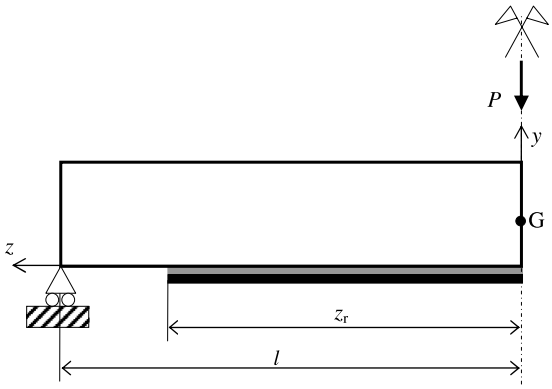

Fig. 2. A FRP reinforced beam in a three point bending configuration. Symmetry is exploited to study only half of the structure.

beam with a rectangular cross section (Fig. 1) reinforced by an FRP strip at its bottom. In the following, the quantities with subscript b refer to the beam to be strengthened, the quantities with subscript a refer to the adhesive layer and the ones with subscript r to the reinforcement. Thus E_b, E_r, G_a are the Young's moduli of the beam, of the reinforcement and the shear modulus of the adhesive; h_b, h_r, h_a are their respective thicknesses; t_b and $t_r = t_a$ their widths. The mechanical percentage of reinforcement is therefore:

$$\rho = \frac{E_r h_r t_r}{E_b h_b t_b}. \tag{1}$$

Usually, the thicknesses of the adhesive layer and of the FRP strip are one or two orders of magnitude smaller than the beam height. Hence, when computing the centre of gravity and the moment of inertia of the reinforced section, their ratio can be neglected if compared to unity. Thus the position y_G of the centre of gravity of the reinforced section (with respect to the bottom of the beam) and its moment of inertia (with respect to the x_G axis) read (Fig. 1):

$$y_G = \frac{h_b}{2\,(1+\rho)} \qquad I = \frac{1+4\rho}{1+\rho} I_b \tag{2}$$

where $I_b = t h_b^3/12$ is the moment of inertia of the plain beam section.

Let us consider a three point bending (TPB) geometry (Fig. 2). The beam span is $2l$ and P is the concentrated load. The length of the FRP strip (i.e. the bond length) is $2z_r$. If z is the axial coordinate with origin at the beam mid-span, in the left side of the beam the shear force is $T = +P/2$ and the bending moment is $M = -P(l-z)/2$. Therefore, according to the well-known equivalent beam model, the horizontal normal stress $(\sigma_z)_r$ in the reinforcement and the

shearing stress $(\tau_{yz})_a$ in the adhesive layer are:

$$\sigma_r = \frac{3\rho}{1+4\rho}\frac{P}{h_r t_r}\frac{l}{h_b}\left(1-\frac{z}{l}\right), \quad 0 < z < z_r \tag{3}$$

$$\tau_a = \frac{3\rho}{1+4\rho}\frac{P}{h_b t_r}, \quad 0 < z < z_r \tag{4}$$

where the subscripts z and yz have been dropped for the sake of clarity.

In order to study the edge delamination of the FRP strip, a simple stress based failure criterion can be set assuming that debonding occurs whenever the shearing stress in the adhesive layer τ_a reaches its critical value τ_c. It should be observed that τ_a does not depend on the length of the reinforcement z_r and, therefore, the critical load is independent too. Since this is clearly in contrast with the experimental data, we conclude that the stress criterion applied to the EB model is too poor to provide an even rough estimate of the failure load.

On the other hand, an energy failure criterion can be set by using the LEFM concept of the strain energy release rate. For fixed load conditions, the strain energy release rate is provided by the derivative of the strain energy of the whole structure with respect to the crack area A given by the product of the crack length a times its width t_r. Hence, the equivalent beam model yields:

$$G = \frac{\mathrm{d}\Phi}{\mathrm{d}A} = \frac{1}{t_r}\left[\frac{M^2}{2E_b I_b} - \frac{M^2}{2E_b I}\right]_{z=z_r}. \tag{5}$$

Applying Eq. (2), we obtain the following estimates of the SERR:

$$G = \frac{9\rho}{2\,(1+4\rho)}\frac{P^2\,(l-z_r)^2}{t_r t_b h_b^3 E_b}. \tag{6}$$

According to LEFM, debonding occurs whenever the SERR reaches its critical value G_c, i.e. the fracture energy. It is worth observing that the SERR (6) strongly depends on the reinforcement length z_r. Consequently, the debonding load provided by the LEFM criterion and Eq. (6) decreases as the bond length decreases: this finding is coherent with experimental data and with the observed instability (brittleness) of the debonding mechanism. In the next section, it will be shown that Eq. (6) is a limit value of the SERR estimate obtained by means of a more refined model.

3. Shear lag model

With respect to the equivalent beam, a more refined model can be achieved by assuming that the cross sections remain planar after deformation only inside the beam to be strengthened. In fact it is argued that, since the main duty of the adhesive layer is to transfer stresses from the beam to the FRP reinforcement by means of tangential stresses, the shearing stress and strain inside the adhesive layer have to be explicitly taken into account to have a more accurate description of the geometry analysed. On the other hand, for the sake of simplicity, no normal (peeling) stresses are considered within its thickness, i.e. the adhesive layer acts as a shear lag (SL). Note that this is a common assumption in structural mechanics problems: see, for instance, [25] for the pull-out problem or [26] for tubular joints.

The assumption of planar cross sections reads:

$$w_b\,(y,z) = w_{b0}\,(z) + \varphi_b\,(z)\,y \tag{7}$$

where w_b is the axial displacement of the beam points, φ_b is the rotation of the cross section at the distance z from the mid-span and w_{b0} is the axial displacement of the points at the bottom of the beam. Denoting by ε_b and ε_r the dilations of the beam points and of the reinforcement and by γ_a the shearing strain of the adhesive, the assumption of a linear elastic behaviour for all the materials composing the structure yields:

$$\sigma_b = E_b\varepsilon_b = E_b\left(\frac{\mathrm{d}w_{b0}}{\mathrm{d}z} + \frac{\mathrm{d}\varphi_b}{\mathrm{d}z}y\right) = E_b\,(\varepsilon_{b0} + \chi_b y) \tag{8}$$

$$\tau_a = G_a\gamma_a = G_a\frac{w_{b0}-w_r}{h_a} = \frac{G_a}{h_a}\delta \tag{9}$$

$$\sigma_r = E_r\varepsilon_r = E_r\frac{\mathrm{d}w_r}{\mathrm{d}z} \tag{10}$$

where χ_b is the beam curvature, ε_{b0} is the dilation at the beam intrados and $\delta = w_{b0} - w_r$ is the relative displacement between the FRP and the beam soffit.

Although it is written in terms of adhesive stiffness and thickness, the task of Eq. (9) is to take into account the interface compliance, which, especially for concrete beams, is the sum of two contributions: the adhesive layer itself and the external cover of the beam. It is worth noting that the second term may be the prevailing contribution in real applications due to the small thickness of the adhesive (about 0.2–0.5 mm), whereas the thickness of the external layer of concrete contributing to interface compliance could be estimated to be about 25–30 mm wide [24]. However, for the sake of clarity, we will keep on referring to the symbols used in Eq. (9).

The normal stress distribution along each cross section has to be equivalent to the axial force (which is equal to zero) and with the bending moment M. In formulae:

$$\int_0^{h_b}\sigma_b t_b\,\mathrm{d}y + \sigma_r t_r h_r = 0 \tag{11}$$

$$\int_0^{h_b}\sigma_b y t_b\,\mathrm{d}y = M. \tag{12}$$

Substituting Eqs. (8) and (10) into Eqs. (11) and (12), we get two algebraic equations from which it is possible to express the strain at the bottom of the beam and the beam curvature as functions of the strain in the FRP strip:

$$\varepsilon_{b0} = \frac{3P}{t_b h_b^2 E_b}(l-z) - \rho\varepsilon_r \tag{13}$$

$$\chi_b = \frac{6\rho\varepsilon_r}{h_b} - \frac{6P}{t_b h_b^3 E_b}(l-z). \tag{14}$$

It is now convenient to express all the unknown variables as functions of δ, the relative displacement between the FRP and the beam intrados. Deriving the expression $\delta = w_{b0} - w_r$ and using Eq. (13), we get:

$$\varepsilon_r = \frac{1}{1+4\rho}\left[\frac{3P\,(l-z)}{t_b h_b^2 E_b} - \frac{\mathrm{d}\delta}{\mathrm{d}z}\right]. \tag{15}$$

The longitudinal equilibrium equation of the FRP strip is:

$$h_r\frac{\mathrm{d}\sigma_r}{\mathrm{d}z} + \tau_a = 0. \tag{16}$$

Deriving Eq. (15) and substituting the result into Eq. (16) together with Eqs. (9) and (10), we get the final governing second order differential equation in the unique unknown variable δ:

$$\frac{\mathrm{d}^2\delta}{\mathrm{d}z^2} - \frac{G_a\,(1+4\rho)}{E_r h_r h_a}\delta = -\frac{3P}{t_b h_b^2 E_b}, \quad 0 < z < z_r. \tag{17}$$

Boundary conditions are needed to solve the differential equation (17). For symmetry reasons, we set to zero the relative displacement between the beam and the reinforcement at the mid-span. On the other hand, at the edge of the reinforcement, the FRP is unloaded and, therefore, ε_r is null. Hence, by means of Eq. (15), the boundary conditions read:

$$\delta = 0, \quad \text{if } z = 0 \tag{18a}$$

$$\frac{\mathrm{d}\delta}{\mathrm{d}z} = \frac{3P}{t_b h_b^2 E_b}(l-z_r), \quad \text{if } z = z_r. \tag{18b}$$

Before solving the differential equation (17), it is interesting to observe that, if the stiffness G_a/h_a of the adhesive layer tends to infinity, the solution tends to $\delta = 0$, i.e. to the solution provided by the EB model, which is in fact characterised by planar reinforced cross sections. Observe that, however, $\delta = 0$ is the solution (for $G_a/h_a \to \infty$) except in the neighbourhood of the end of the reinforcement where the second derivative of δ becomes unbounded to accomplish the boundary condition (18b). From a mathematical point of view, therefore, we expect the rising of a boundary layer close to $z = z_r$, i.e. a region where the solution strongly varies.

The solution of Eq. (17) together with the boundary conditions (18) yields:

$$\delta = \frac{3Pl^2}{t_b h_b^2 E_b} \frac{f_\tau(\beta, \zeta, \zeta_r)}{\beta^2} \tag{19}$$

f_τ is a dimensionless function given by:

$$f_\tau(\beta, \zeta, \zeta_r) = 1 + \frac{\beta(1-\zeta_r)\sinh(\beta\zeta) - \cosh[\beta(\zeta_r - \zeta)]}{\cosh(\beta\zeta_r)} \tag{20}$$

where ζ and ζ_r are respectively the axial coordinate and the reinforcement length normalised with respect to the beam half-span: $\zeta = z/l$ and $\zeta_r = z_r/l$. β is a dimensionless parameter defined as:

$$\beta^2 = \frac{G_a l^2 (1+4\rho)}{E_r h_r h_a}. \tag{21}$$

By using the relationships (9) and (15) and deriving the solution (19), we obtain the normal stress in the FRP strip and the shearing stress in the adhesive layer:

$$\sigma_r = \frac{3\rho}{1+4\rho} \frac{P}{t_r h_r} \frac{l}{h_b} f_\sigma(\beta, \zeta, \zeta_r) \tag{22}$$

$$\tau_a = \frac{3\rho}{1+4\rho} \frac{P}{t_r h_b} f_\tau(\beta, \zeta, \zeta_r) \tag{23}$$

with f_τ given by Eq. (20) and:

$$f_\sigma(\beta, \zeta, \zeta_r) = (1-\zeta) - \frac{\beta(1-\zeta_r)\cosh(\beta\zeta) + \sinh[\beta(\zeta_r - \zeta)]}{\beta\cosh(\beta\zeta_r)}. \tag{24}$$

First of all it is worth noting that, if $G_a/h_a \to 0$ (i.e. $\beta \to 0$), both functions f_τ and f_σ vanish and consequently $\tau_a = \sigma_r = 0$. From a physical point of view, this means that, if the interface is infinitely compliant, the FRP remains unloaded and consequently has no strengthening effect upon the beam.

Then, it should be observed that the first addend at the right-hand side of Eqs. (20) and (24) represents the EB model solution, i.e. Eqs. (3) and (4), whereas the second term represents the correction to be added if the compliance of the adhesive layer is taken into account. If the stiffness G_a/h_a tends to infinity (i.e. $\beta \to \infty$), this correction disappears except at the end of the FRP strip, where a strong shearing stress concentration appears. From a mathematical point of view, we can state that, as $\beta \to \infty$, the solution provided by the shear lag model shows a non-uniform convergence to the equivalent beam model solution.

Eqs. (22) and (23) are plotted respectively in Figs. 3 and 4 with reference to a three point bending concrete beam strengthened by an FRP strip of different lengths. The geometrical and material values are as follows: $l = 500$ mm; $h_b = 120$ mm, $h_a = 4$ mm, $h_r = 1.6$ mm; $t_r = t_b = 100$; $E_b = 30$ GPa, $G_a = 0.72$ GPa, $E_r = 160$ GPa; $P = 70$ kN. The dashed lines represent the equivalent beam model solution, which is independent of ζ_r. Fig. 3 shows that the stress in the FRP provided by the shear lag model is always lower than the stress provided by the equivalent beam model. The opposite happens for the shearing stress, for which the SL model provides values much higher than the ones provided by the EB model (except close to the mid-span, where the shearing stress vanishes). It is evident that, with respect to the simpler beam model, the shear lag model is able to catch the shearing stress concentration at the edge of the FRP strip, which is the cause of the FRP debonding. The stress concentration tends to increase as the bond length decreases up to a certain value, as clearly shown in Fig. 4. On the other hand, beyond a certain distance from the mid-span and the edge of the reinforcement, the two solutions actually coincide.

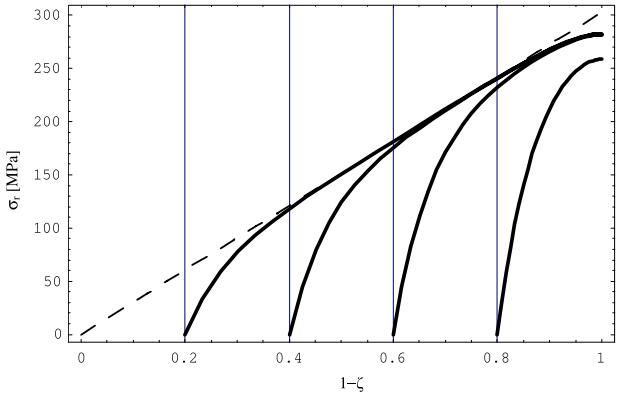

Fig. 3. Horizontal normal stress in the FRP versus the axial coordinate normalised with respect to the beam half span. The thick lines refer to a bonded length ζ_r equal to 0.8, 0.6, 0.4, 0.2 from left to right. The dashed line represents the equivalent beam model solution.

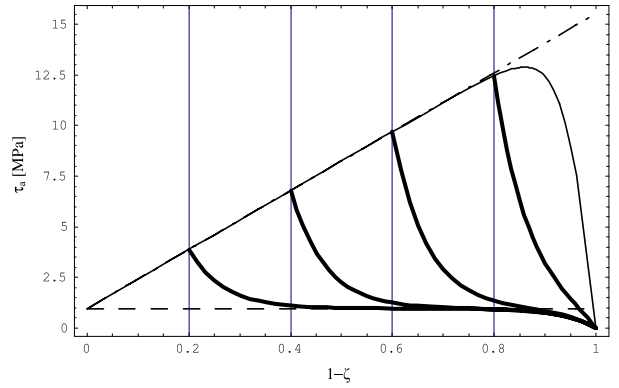

Fig. 4. Shearing stress in the adhesive layer versus the axial coordinate normalised with respect to the beam half span. The thick lines refer to a bonded length ζ_r equal to 0.8, 0.6, 0.4, 0.2 from left to right. The thin line is the envelope of the maximum values of the shearing stress, and the dot-dashed line is its approximate value according to Eq. (51). The dashed line represents the equivalent beam model solution.

Eventually, it is worth observing that, if the geometry under consideration (Fig. 2) is dealt with as a two-dimensional elastic problem, the shearing stress in the adhesive layer at the edge of the FRP strip is zero. In other words, there exists a shearing stress concentration close to the reinforcement edge, but boundary conditions force the shearing stress to vanish at the FRP edge. This peculiar behaviour is not caught by the shear lag assumption (i.e. Eq. (9)) used here, so that failure criteria based on the shearing stress distribution Eq. (23) may appear somehow arbitrary. Nevertheless, in [9] it has been shown that the strain energy release rate estimate provided by the SL model is close to the one obtained by higher order models (where the adhesive is actually modelled by a 2D elastic medium), thus justifying the use of the SL assumption throughout the rest of the present paper.

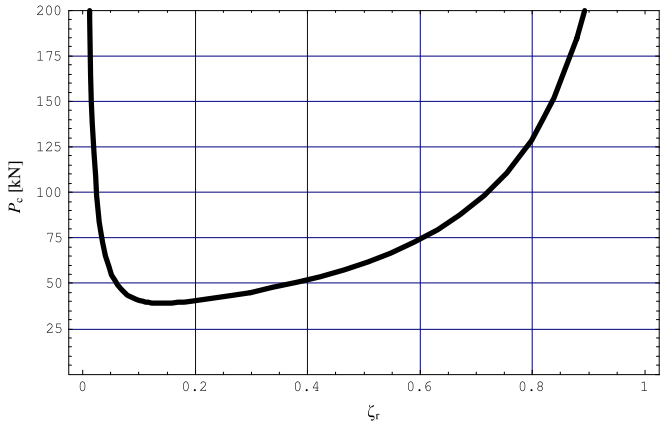

Fig. 5. Failure load versus relative reinforced length according to the stress-based failure criterion.

4. Stress failure criterion

The maximum value of the shearing stress in the adhesive layer is attained at the end of the reinforced zone, i.e. for $\zeta = \zeta_r$. From Eqs. (20) and (23):

$$\tau_{\max} = \frac{3\rho}{1+4\rho}\frac{P}{t_r h_b} f_{\tau\,\max}(\beta, \zeta_r) \tag{25}$$

$$f_{\tau\,\max}(\beta, \zeta_r) = 1 + \beta(1-\zeta_r)\tanh(\beta\zeta_r) - \operatorname{sech}(\beta\zeta_r). \tag{26}$$

Eq. (25) is plotted in Fig. 4 (thin line): it represents the envelope of the maximum shearing stress varying the relative reinforcement length. Assuming that the load causing delamination is attained when the maximum shearing stress $\tau_{\max}$ reaches the interfacial strength τ_c, that is:

$$\tau_{\max} = \tau_c \tag{27}$$

the critical load P_c is then provided by the following expression:

$$P_c = \frac{1+4\rho}{3\rho}\frac{\tau_c t_r h_b}{f_{\tau\,\max}(\beta, \zeta_r)}. \tag{28}$$

For the same geometry considered in the previous section, the critical load vs. bond length is plotted in Fig. 5 for a τ_c value equal to 7.2 MPa [27]. Since, according to the present model, the debonded portion of the FRP strip becomes stress-free, the plot in Fig. 5 can be interpreted as either the graph of the critical loads for different initial lengths of the FRP strip, or the diagram of the load during the debonding process for a given initial FRP strip length. In the latter case, it is interesting to observe that, if the process is load-controlled, the debonding process is unstable until the reinforcement length is much shorter than the beam length (about 20%). In that case, the model predicts a load increase to have a further debonding. However, it is worth observing that the final ascending branch of the curve in Fig. 5 for $\zeta_r \to 0^+$ is not observed in experimental tests, where delamination ends with the complete detachment of the FRP strip from the beam intrados. As we shall see later, this behaviour is due to the snap–back and snap-through instabilities.

Although able to catch the brittleness of the debonding failure, the stress failure criterion (28) shows some shortcomings. In fact, for low adhesive compliances ($\beta \to \infty$), the critical load provided by Eq. (28) vanishes, a result which is physically meaningless. From a mathematical point of view, this is due to the non-uniform convergence of the shearing stress field provided by the SL model to the EB model: at the edge of the FRP and for $\beta \to \infty$, instead of converging to Eq. (4), the maximum shearing stress (25) tends to infinity, forcing the failure load (28) to zero. Thankfully, this drawback does not characterise the energetic failure criterion that will be addressed in the next section within the framework of the LEFM and of the SL model. This nice feature of the energy approach is not surprising at all, since the remarkable brittleness of the debonding phenomenon fully justifies the use of LEFM.

5. Energy failure criterion

Under a fixed grip condition, the strain energy of a structure usually decreases when a crack embedded in the same structure grows, since the global compliance increases. Hence, a crack will start growing if the amount of the energy release due to the crack increment is equal to or larger than the energy necessary to create the new fracture surface. This energy balance is the basic concept of LEFM: fracture occurs whenever the strain energy release rate G (SERR) reaches its critical value, the fracture energy G_c:

$$G = G_c. \tag{29}$$

G_c is a property of the material or, as in the present case, of the interface. On the other hand, the strain energy release rate can be evaluated following two different strategies, i.e. a global approach or a local approach. According to the former approach, one has to evaluate the strain energy Φ of the whole structure. Then, it can be proven that:

$$G = +\frac{\mathrm{d}\Phi}{\mathrm{d}A}\bigg|_{\text{fixed load}} = -\frac{\mathrm{d}\Phi}{\mathrm{d}A}\bigg|_{\text{fixed displacement}} \tag{30}$$

that is, the SERR is the derivative of the strain energy with respect to the crack area A at fixed load or its opposite for fixed displacement. In the paper by Rabinovitch [9], the SERR was evaluated by means of Eq. (30) and according to different structural models of increasing complexity, namely the EB model, the one-parameter elastic foundation beam model (i.e. the SL model), the two-parameter elastic foundation beam model and a higher order model.

However, the computation of the derivative of the strain energy Φ is so laborious that Rabinovitch [9] had to use a numerical approximation even in the relatively simple case of the shear lag model of a TPB reinforced beam. Actually, he applied the Virtual Crack Extension Method to obtain the following estimate of the SERR:

$$G \approx +\frac{\Delta\Phi}{\Delta A}\bigg|_{\text{fixed load}} \tag{31}$$

that is, he replaced the derivative with the related finite difference. On the other hand, when the stress-displacement field at the crack tip is known, a local approach is more effective and will be set forward and used in what follows. In Appendix A it will be verified that the two approaches yield the same result for the geometry of interest.

According to the local approach, the SERR has to be computed by the application of Clapeyron's theorem to the crack closure work. Let us consider two schemes (Fig. 6) under fixed grip condition: the former (Fig. 6a) with an interfacial crack of length Δa and width t_r and the latter one without (Fig. 6b). Clapeyron's theorem states that the strain energy is one half of the product of the shearing stress τ_a (closed crack) times the relative displacement w_{rel} between the crack lips (open crack):

$$(\Delta\Phi)_{\text{closure}} = \frac{t_r}{2}\int_{z_r}^{z_r+\Delta a} \tau_a(z, z_r+\Delta a)\, w_{\text{rel}}(z, z_r)\, \mathrm{d}z \tag{32}$$

where we emphasised that the stress and displacement fields depend on the longitudinal coordinate z as well as on the reinforcement lengths (respectively $z_r + \Delta a$ and z_r). More in detail, the relative displacement is given by the difference between the displacement of the beam intrados and the displacement at the edge of the FRP strip, which does not depend on z since the

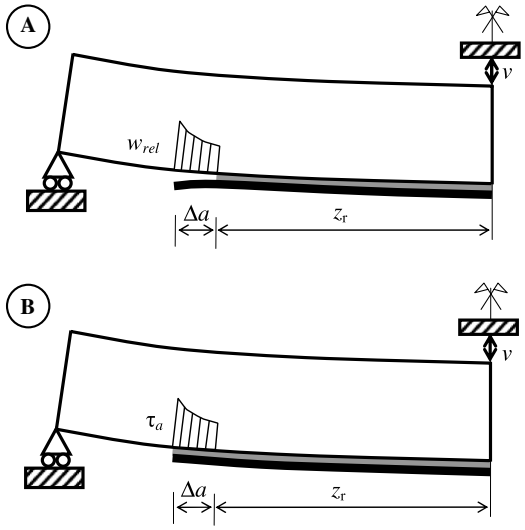

Fig. 6. Crack (Δa) closure work under fixed grip condition. Open crack (A): $w_{\rm rel}$ is the relative displacement between crack lips. Closed crack (B): τ_a is the shearing stress acting along the crack lips.

unbonded part of the FRP is undeformed:

$$w_{\rm rel}\,(z, z_r) = w_{b0}\,(z, z_r) - w_r\,(z = z_r, z_r)\,. \tag{33}$$

Since, for $h_a \neq 0$, the integrand functions are not singular, the mean value theorem can be applied leading to:

$$(\Delta\Phi)_{\rm closure} = \frac{t_r}{2}\Delta a\tau_a\,(\bar{z}, z_r + \Delta a)\,w_{\rm rel}\,(\bar{z}, z_r) \tag{34}$$

where $\bar{z}$ is a point lying within the interval of integration, i.e.: $z_r \leq \bar{z} \leq z_r + \Delta a$. Now, by means of Eq. (30) at fixed displacement:

$$\begin{aligned} G &= -\lim_{\Delta A\to 0}\frac{(\Delta\Phi)_{\rm opening}}{\Delta A} \\ &= \lim_{\Delta a\to 0}\frac{\tau_a\,(\bar{z}, z_r + \Delta a)\,w_{\rm rel}\,(\bar{z}, z_r)}{2} \\ &= \frac{\tau_a\,(z_r, z_r)\,w_{\rm rel}\,(z_r, z_r)}{2} \end{aligned} \tag{35}$$

where $\Delta A = t_r \times \Delta a$ is the crack surface and the last equality holds since, as $\Delta a \to 0$, all the independent variables collapse onto the value z_r. But this means that the SERR is half of the product of the shearing stress at the FRP edge, i.e. the maximum shearing stress $\tau_{\rm max}$, and the corresponding relative displacement $\delta_{\rm max}$, which, in its turn, can be expressed as a function of $\tau_{\rm max}$ by means of the constitutive Eq. (9). Hence:

$$G = \frac{\tau_{\rm max}^2}{2G_a}h_a \tag{36}$$

Eq. (36) plays a key role since it bridges the energetic approach with the stress analysis. It is very similar, also for the way it was derived by, to Irwin's relationship between the strain energy release rate and the stress-intensity factor K_I : $G = K_I^2/E$. As well known, Irwin's relationship holds for a crack propagating (under mode I conditions) within a homogeneous medium of Young's modulus E. Irwin's formula represents the key to relate the global energetic analysis by Griffith with the local stress field analysis due to Westergaard. Analogously, Eq. (36) provides the strain energy release rate as a function of the maximum shearing stress for an interfacial crack propagating (under mode II conditions) within a shear lag whose shear stiffness is G_a/h_a. Although in its derivation we made reference to the TPB geometry, the argument we set is general: therefore we claim that Eq. (36) is a result valid for all the shear lag models. To the authors' knowledge, Eq. (36) has never been clearly stated up to now. In [28] the same relation has been verified (not proven) by separately computing the SERR and the maximum shearing stress for a given geometry, namely the push–pull shear test: this is a validation of the general result (36). Moreover, it is worth noting that Leung [28] obtained also a relationship similar to Eq. (36) considering a linear softening: his result makes the extension of the present approach to softening interfaces very attractive. However it will not be considered here since it is beyond the scope of the present paper.

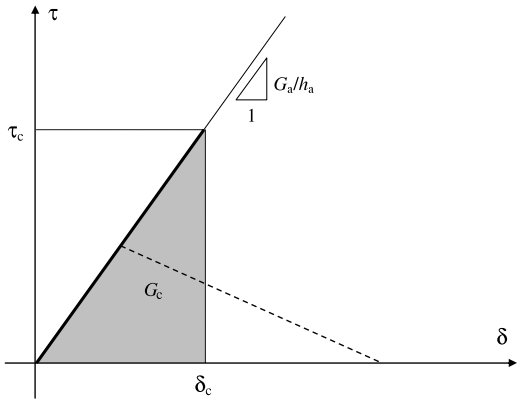

Fig. 7. Thick line: elastic-purely brittle constitutive law for the interface; the grey area represents the fracture energy. Dashed line: linear softening cohesive law with the same fracture energy of the elastic-purely brittle law.

Eq. (36) shows that the stress (27) and energy (29) failure criteria yield the same results as long as the following relation holds between the critical values τ_c and G_c:

$$\tau_c = \sqrt{\frac{2G_cG_a}{h_a}}. \tag{37}$$

The value of τ_c provided by Eq. (37) can be seen as an effective interfacial shear strength, so that the conventional strength-based approach can be employed to give the same result of the energy-based fracture criterion. It allows one to bypass the complex energetic analysis performed by several authors, e.g. [9,25].

Eq. (37) shows also that the LEFM criterion (29) corresponds to assume an elastic-purely brittle constitutive law for the interface (Fig. 7). In such a case, in fact, the area beneath the straight line is $\tau_c \times \delta_c/2$, δ_c being the critical relative displacement. Since the slope of the line is G_a/h_a and the area is equal to G_c, Eq. (37) follows straightforwardly. Although this easy proof holds only for critical conditions, Eq. (37) is a further confirmation of the general result (36).

Let us now apply Eq. (36) to the geometry we are interested in, that is, the TPB of a FRP-reinforced beam. Since the maximum shearing stress is provided by Eq. (25), the following estimates of the SERR is achieved:

$$G = \frac{9\rho^2}{2\,(1+4\rho)^2}\left(\frac{P}{t_rh_b}\right)^2\frac{h_a}{G_a}f_{\tau\,\rm max}^2\,(\beta, \zeta_r)\,. \tag{38}$$

By some manipulations, Eq. (38) can be recast in the following form:

$$G = \frac{9\rho}{2\,(1+4\rho)}\frac{P^2l^2}{t_rt_bh_b^3E_b}\frac{f_{\tau\,\rm max}^2\,(\beta, \zeta_r)}{\beta^2}. \tag{39}$$

It is worth considering explicitly the two limit cases: $\beta \to \infty$ and $\beta \to 0$. By means of Eq. (26) we can prove that:

$$\lim_{\beta\to\infty}\frac{f_{\tau\,\rm max}\,(\beta, \zeta_r)}{\beta} = 1 - \zeta_r \tag{40a}$$

$$\lim_{\beta\to 0}\frac{f_{\tau\,\rm max}\,(\beta, \zeta_r)}{\beta} = 0. \tag{40b}$$

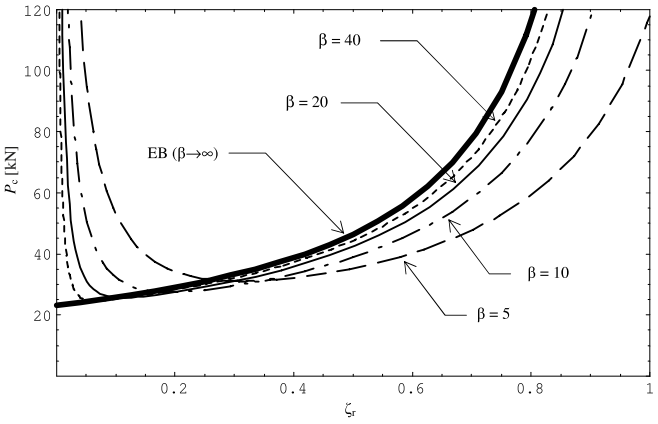

Fig. 8. Debonding load versus relative bond length ζ_r according to the energy-based failure criterion. The thick line corresponds to the predictions obtained by the EB model, the thin lines to the SL model for different values of the parameter β.

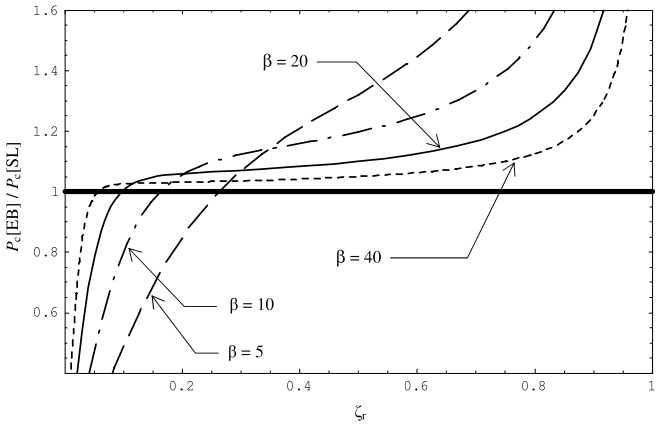

Fig. 9. Energy-based failure criterion: Ratio between the critical load estimates based on the EB and SL models for different values of β versus the relative bond length ζ_r.

Eq. (40a) clearly shows that, as the compliance of the shear lag vanishes (i.e. $\beta \to \infty$), the SERR estimate (39) provided by the SL model tends to the estimate (6) provided by the EB model. This positive feature is peculiar to the energy approach, since, as pointed out in the previous section, the maximum shearing stress (25) tends to infinity instead of tending to the EB value (4) as $\beta \to \infty$. This difference between the two approaches is due to the local character of the strength-based criterion (27), opposite to the global nature of the energy-based one (29).

On the other hand, Eq. (40b) shows that the SERR vanishes for an infinitely compliant interface, which is reasonable since, as noted above, in such a case the FRP strip has no strengthening effect.

According to LEFM criterion (29), the critical load is then provided by:

$$P_c = \sqrt{\frac{1+4\rho}{\rho}}\sqrt{2t_r t_b h_b E_b G_c}\,\frac{h_b}{3l}\,\frac{\beta}{f_{\tau\,\max}(\beta,\zeta_r)}. \tag{41}$$

If the material and the geometry of the beam cross section are assigned, Eq. (41) shows that the critical load decreases as the mechanical percentage of reinforcement ρ or the beam slenderness $2l/h_b$ increase, while, at constant ρ, it increases with the square root of the strip width t_r. The latter effect is due to the higher energy that has to be dissipated as the bonded zone increases. Finally, the last ratio at the right-hand side of Eq. (41) provides the strengthening effect of the relative bond length ζ_r.

It is worth observing that both analytical models as well as experimental data have shown that an increment of ρ yields an increase in the load causing IC-debonding. It means that the mechanical percentage of reinforcement ρ affects the edge and the IC debonding mechanisms in the opposite way, i.e. the larger is ρ, the higher is the load causing IC debonding, the lower is the load corresponding to edge debonding and vice-versa.

Eq. (41) is plotted in Fig. 8 assuming a fracture energy G_c equal to 65 J/m^2 [9], which corresponds to the concrete fracture energy, since the debonding crack typically runs under the concrete skin. The values of the other geometrical and mechanical quantities are the same given in Section 3. We let the interface stiffness G_a/h_a vary and, consequently, the parameter β: hence the different curves in Fig. 8 refer to different values of β. It is evident that, as the shear lag compliance diminishes ($\beta \to \infty$), the critical load (41) provided by the SL model tends to coincide with the one obtained by the EB model through Eqs. (6) and (29). This result is of particular interest since, in some papers (e.g. [10]), it is stated that the EB model provides a very good estimates of the SERR if compared to more refined models such as the SL one, whereas other researchers (e.g. [9]) account for examples where the difference between the SERR estimates is of major importance. Since we obtained the SERR analytically (Eq. (39)), the answer to this problem is straightforward: it depends on the parameter β. For high β values, the difference between the SERR estimates will be irrelevant whereas will be significant if β is not so high, as in the case considered later (Table 1).

A second important consideration related to Fig. 8 is that, for usual values of the relative reinforcement length (i.e. 70% or higher), the EB model provides an overestimate of the failure load if compared to the more refined shear lag model. This is clearly represented in Fig. 9 where the ratio between the critical load provided by the EB and SL model is plotted vs. the relative reinforcement length and for different values of the parameter β. Note that the ratio depends only on the parameter β and the relative bond length ζ_r:

$$\frac{(P_c)_{\mathrm{EB}}}{(P_c)_{\mathrm{SL}}} = \frac{f_{\tau\,\max}(\beta,\zeta_r)}{\beta\,(1-\zeta_r)}. \tag{42}$$

It is therefore evident that the uncritical application of the EB model is potentially dangerous. Finally, it is worth observing that, according to the SL model, an ascending branch in the critical load plot (Fig. 8) for $\zeta_r \to 0^+$ has to be expected, a trend which is not caught by the EB model.

6. Post-peak response and instabilities in the debonding process

In the previous sections we analysed the conditions for the onset of the debonding mechanism. Aim of the present section is to analyse the structural behaviour during the debonding process.

Since we assumed an elastic-purely brittle behaviour of the interface, the debonded part of the FRP is unloaded: it means that a growth of the interfacial crack is equivalent to a decrement of the reinforcement length. Therefore Fig. 8 shows not only that the critical load decreases as the length of the FRP strip diminishes but also that, in the first part of the debonding process, the failure load necessary to have a further debonding of the reinforcement decreases. This means that, if load-controlled, the delamination process is clearly unstable. And what about if the test is under displacement control?

To provide an answer to the previous question it is necessary to compute the displacement of the point where the load is applied, i.e. the deflection at the mid-span. This value may be computed following two different strategies: by integrating the deformation functions (13)–(15) or by means of Castigliano's theorem. The latter way is by far more elegant and effective. In fact, since we

Table 1
Comparison between the main physical quantities obtained according to the different models and to a numerical analysis. Where not explicitly given, the values are taken from Rabinovitch [9].

	Equivalent beam model	Shear lag model (one-parameter elastic foundation model)	Two-parameter elastic foundation model	Finite element analysis
$(\tau_a)_{\max}$ [MPa]	0.969 [Eq. (4)]	3.880 [Eq. (25)]	3.843	3.266
$(\sigma_a)_{z=z_r}$ [MPa]	–	–	1.326	from −4.852 to 13.10
G [J/m^2]	23.55 [Eq. (6)]	41.83 [Eq. (39)]	42.78 [Eq. (48)]	–
$v_{\max}$ [mm]	2.820 [Eq. (47), $\beta \to \infty$]	2.832 [Eq. (47)]	2.820	2.818

already know the SERR, in order to achieve the strain energy Φ of (half of) the whole structure, we simply need to integrate Eq. (30) at fixed load. Since $dA = t_r da = -t_r dz_r$:

$$\Phi_{\text{No FRP}} - \Phi = t_r \int_0^{z_r} G(z_r)\ dz_r \tag{43}$$

where $\Phi_{\text{No FRP}}$ is the strain energy of the beam without reinforcement. Upon substitution of Eq. (36) into Eq. (43), we get:

$$\Phi = \Phi_{\text{No FRP}} - \frac{t_r h_a}{2G_a} \int_0^{z_r} \tau_{\max}^2(z_r)\ dz_r \tag{44}$$

$\Phi_{\text{No FRP}}$ is known from classical beam theory, whereas $\tau_{\max}$ is provided by Eq. (25). Therefore:

$$\Phi = \frac{P^2 l^3}{2E_b t_b h_b^3} \left\{ 1 - \frac{9\rho}{1+4\rho} \int_0^{\zeta_r} \left[\frac{f_{\tau\,\max}(\beta, \zeta_r)}{\beta} \right]^2 d\zeta_r \right\}. \tag{45}$$

According to Castigliano's theorem, the displacement of the point where the load is applied is provided by the derivative of the strain energy Φ with respect to the load P:

$$v_{\max} = 2\frac{d\Phi}{dP} \tag{46}$$

where the coefficient 2 appears since Φ is the strain energy contained in half of the beam. Hence:

$$v_{\max} = \frac{2l^3}{E_b t_b h_b^3} \left\{ 1 - \frac{9\rho}{1+4\rho} \int_0^{\zeta_r} \left[\frac{f_{\tau\,\max}(\beta, \zeta_r)}{\beta} \right]^2 d\zeta_r \right\} \times P. \tag{47}$$

It is worth pointing out that the expression within brackets in Eq. (47) is always less than unity. It means that, at fixed load, the mid-span deflection of a reinforced beam is always lower than the mid-span deflection of the corresponding beam without the FRP strip. More in detail, the SL model provides for the mid-span deflection an estimate (i.e. Eq. (47)) which is comprised between the deflection of the beam without reinforcement (when $\beta \to 0$ and Eq. (40b) holds) and the deflection of the strengthened beam evaluated by the EB model (when $\beta \to \infty$ and Eq. (40a) holds).

The integral at the right-hand side of Eqs. (45) and (47) can be easily computed analytically. However, since its expression is rather long, the explicit result is given in Appendix B.

Once the mid-span deflection is computed, the load vs. deflection curve during edge debonding of the FRP can be easily plotted. We just need to substitute Eq. (41) into Eq. (47). Then Eqs. (41) and (47) can be seen as the equation of a curve in the plane $(P, v_{\max})$ defined parametrically by means of ζ_r. The typical shape of such a curve is shown in Fig. 10, where, for the sake of clarity, also the straight lines corresponding to the beam configurations with a completely bonded FRP strip and without reinforcement have been drawn. Coherently with the assumed linear elastic-purely brittle behaviour of the interface, the load vs. deflection curve is represented by a straight line up to debonding initiation. Then softening begins with a positive slope in the first part of the debonding process. This means that a snap–back instability occurs under displacement control: the curve in Fig. 10 could be actually captured only if the failure process were controlled by the interfacial

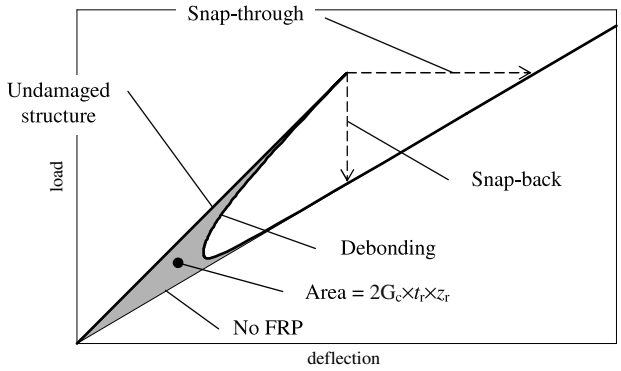

Fig. 10. Typical load vs. deflection curve for a TPB beam undergoing an edge debonding failure and related instabilities.

crack length, i.e. ζ_r. When the relative reinforcement length drops to about 20%, the load reverts increasing along with the deflection. Finally, the curve tends to the straight line describing the linear elastic behaviour of the un-reinforced structure and global detachment of the FRP strip is virtually achieved at infinite load.

A first comment is that the area comprised between the load vs. deflection curve and the straight line characterising the un-reinforced structure represents the energy dissipated in the debonding process, i.e. the product of the interfacial fracture energy G_c times the bonded area $2z_r \times t_r$. A second comment is about the instabilities: as the debonding process initiates, a deflection jump occurs if the test is load-controlled (snap-through); on the other hand, a sudden decrease of the load is to be expected if the test is displacement-controlled (snap–back). The snap–back and snap-through are represented by the dashed segments in Fig. 10.

Although the scope of the present paper is mainly the presentation of a theoretical approach to the edge debonding mechanism, it is worth commenting shortly the differences between the analytical curve shown in Fig. 10 and the curves that may be obtained in experimental tests. First of all, matching with experimental data is expected only if the edge debonding is the failure mechanism to which the lowest failure load corresponds: according to Eq. (41), edge debonding happens more likely for high percentages of mechanical reinforcement and/or low relative reinforcement lengths. After debonding initiates, the softening curve provided by the present approach is realistic only if no other failure mechanisms take place, i.e. the behaviour of the various components (with the exception of the interface) of the composite structure remain linear elastic. Of course, this rarely occurs in concrete beams where the debonding of the FRP yields the fracturing of lower side of the beam or even final crashing if no steel bars are present inside the beam itself.

A closer matching between theory and experiments is expected for FRP strengthened metallic beams. Preliminary experimental results [29] obtained testing tubular aluminium beams have shown a transition in the failure modes by varying the relative reinforcement lengths: for low ζ_r values, edge debonding preceded buckling of lateral beam walls; the opposite occurred for high ζ_r values. This behaviour is coherent with Eq. (41), although it was

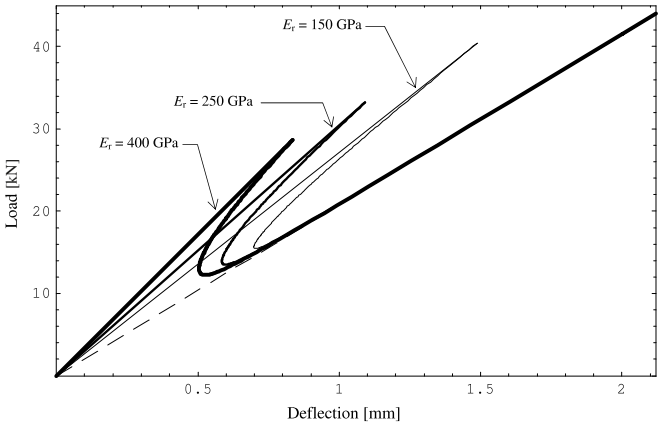

Fig. 11. Load vs. mid-span deflection for different values of the Young's modulus of the FRP: $E_r = 400$ GPa (thick line); $E_r = 250$ GPa (middle line); $E_r = 150$ GPa (thin line). The dashed line corresponds to the stiffness of an un-reinforced beam. The initial relative bond length is set equal to 75%.

obtained for a rectangular cross section. In fact Eq. (41) states that the debonding load strongly decreases while diminishing the bond length, whereas collapse mechanisms taking place at the mid-span (e.g. plastic or buckling collapses) are not affected by this parameter. For what concerns the softening branch of the curve, since the tests were displacement-controlled, a snap back occurred if edge debonding took place. However, the extra amount of energy due to the snap–back instability caused the sudden detachment of the whole FRP strip from the beam, so that the load jump corresponds to the jump between the two straight lines representing the linear elastic behaviour of the reinforced and un-reinforced structures in Fig. 10.

In Fig. 11 the load vs. deflection curves are plotted according to the values given in Section 3, except for what concerns the FRP. We chose a FRP thickness equal to 3 mm and let the Young's modulus E_r of the FRP strip vary according to the following values: 400, 250 and 150 GPa. Furthermore, the initial bond length was assumed equal to 75%. It is seen that the higher is the FRP stiffness, the lower is the debonding failure load and the weaker the snap–back instability. It is worth observing that the area between each curve and the straight line describing the un-reinforced structure is constant and equal to the energy necessary to have a complete detachment of the FRP strip.

Finally, let us consider again the TPB geometry proposed in Section 3, which is the same as considered in [9]. The quantities of major interest are provided in Table 1 according to a finite element analysis (FEA) and to the different models considered herein: the EB model, the SL model (i.e. the one-parameter elastic foundation model) and the two-parameter elastic foundation model. For what concerns the mid-span deflection, all the models provide quite accurate predictions. On the other hand, about the maximum shearing stress, the EB model is completely unreliable, whereas the SL model provide a rather good estimate, which is less then 20% from the numerical value obtained in the FEA. For what concerns the SERR, it is seen that the prediction of the simplest model strongly differs from the SL model estimate (a fact that, as discussed previously, is due to the choice of a relatively high adhesive layer compliance). On the other hand, the SERR estimates provided by the SL model and the two-parameter elastic foundation model are very close. This result validates somehow the assumption of neglecting the peeling stresses in the adhesive layer. Therefore, to summarize, we conclude that the SL model is a reasonable compromise between simplicity and refinement to address the onset of the FRP debonding, at least for the TPB geometry.

About the data in Table 1, it is worth making two more comments. The former is that, although the data corresponding to the SL model actually coincide with the values obtained by Rabinovitch [9], we evaluated the SERR analytically by means of Eq. (36) whereas in [9] the same values were obtained numerically, i.e. applying the Virtual Crack Extension Method (Eq. (31)). The advantage is evident and strongly increases the usefulness of the energetic approach. The latter comment is that the generalisation of Eq. (36) to the two-parameter elastic foundation model is straightforward:

$$G = \left[\frac{\tau_a^2}{2G_a}h_a + \frac{\sigma_a^2}{2E_a}h_a\right]_{z=z_r}. \tag{48}$$

It can be easily checked that Eq. (48) is satisfied by the values (taken from [9]) of the third column of Table 1. In other words, by exploiting the stress field solution, Eqs. (36) and (48) provide the key to bypass the complicated energetic analysis in the case respectively of the one-parameter and two-parameter elastic foundation models. In the authors' opinion, this improvement is one of the most important achievements of the present work.

Finally, we wish to emphasise that Eqs. (36) and (48) hold true if the adhesive layer is modelled as a bed of springs. As observed at the end of Section 3, if the adhesive layer is modelled as a 2D elastic medium, the shearing stress τ_a is zero for $z = z_r$ and Eq. (36) provides a meaningless vanishing SERR. Hence, one may question about the validity of the SERR estimates given by Eqs. (36) and (48) and further analyses in this direction are welcome. At present, however, it may be observed that, by adequately modelling the adhesive layer as a plane elastic medium and by exploiting the J-integral, Rabinovitch [9] obtained, for the same geometrical and material values used in Table 1, a SERR estimate which is only 13% higher than the one obtained by the SL model. Although a single check is not a proof, this result seems to indicate that SERR estimates obtained through Eqs. (36) and (48) are reliable indeed.

7. Dimensionless formulation, size effect and simplified formulae

In order to highlight the size effect upon the edge debonding of the FRP for three point bending beams, it is more convenient to re-write Eq. (41) in terms of dimensionless quantities:

$$\frac{P_c}{E_b h_b^2} = \sqrt{\frac{1+4\rho}{\rho}}\sqrt{\frac{t_r}{h_b}}\sqrt{\frac{t_b}{h_b}}\sqrt{\frac{G_c}{h_b E_b}}\frac{\sqrt{2}}{3\,(l/h_b)}\frac{\beta}{f_{\tau\,\max}(\beta,\zeta_r)}. \tag{49}$$

In such a way, it is evident that, keeping constant the mechanical quantities as well as the geometrical ratios, the critical load is proportional to $(h_b)^{3/2}$. Note that this power law behaviour is typical of LEFM; see, for instance, the case of TPB un-reinforced, notched beams [20,30].

As the structural size varies proportionally, the only dimensionless number that changes at the right hand side of Eq. (49) is:

$$s = \frac{G_c}{h_b E_b}. \tag{50}$$

The dimensionless number s rules the size effect in FRP strengthened beams and plays a role analogous to the brittleness number introduced by Carpinteri [19] for the size effect in notched beams. By dividing the deflection by the beam height, the dimensionless load vs. deflection curves may be plotted for different s values. In Fig. 12, the values of the dimensionless parameters are as follows: the cross section aspect ratios t_r/h_b and t_b/h_b are equal to 0.4; the beam slenderness $2l/h_b$ is equal to 8; the parameter β is equal to 8; finally, for the sake of clarity, a rather high value (i.e. $\rho = 0.5$) of the mechanical percentage of reinforcement was chosen. The set of interfacial crack propagation points, with s equal to constant and by varying the relative reinforcement length, represents a virtual load–deflection path, where point by point the load is always

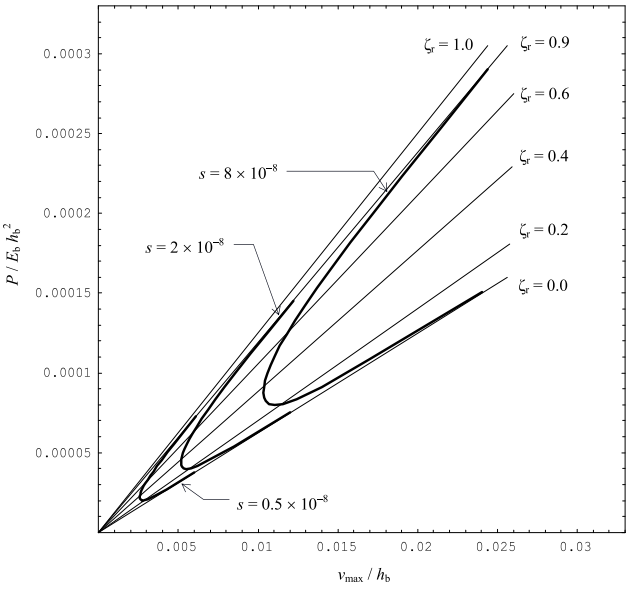

Fig. 12. Dimensionless load of crack instability versus dimensionless deflection. Thin lines refer to linear-elastic behaviour for different relative bond lengths ζ_r. Thick lines represent the softening behaviour during debonding for different values of the dimensionless number s.

that producing crack instability. When the interfacial crack grows, the load of instability initially decreases and the compliance increases, so that the product at the right member of Eq. (47) may result to be either decreasing or increasing. The diagrams in Fig. 12 show the deflection decreasing (with the load) up to a reinforcement length $\zeta_r \cong 0.4$ and then increasing (in discordance with the load) up to $\zeta_r \cong 0.2$. Afterwards, the load reverts to increase along with the deflection, tending to the behaviour of an un-reinforced beam. We wish to emphasise that, for $\zeta_r > 0.4$, the softening branch presents a positive derivative. Such a branch would not be revealed by deflection-controlled testing and the representative point would jump from the upper to the lower softening branch with a discontinuity behaviour.

One may wonder what would change if, instead of an elastic-purely brittle behaviour, a softening cohesive law were considered for the adhesive (e.g. a linear softening, see Fig. 7). At present, we can only argue that this would cause less brittle load vs. deflection curves (Figs. 10–12). However, since in the push–pull shear test the maximum achievable load depends only on the interfacial fracture energy [31,32], it is reasonable to expect that, also for the TPB geometry, the maximum load is not strongly affected by the shape of the function $\tau(\delta)$; on the other hand, an earlier departure from the linear elastic behaviour as well as higher deflections are likely to occur in the case of softening cohesive laws.

Although the present approach is fully analytical, it is argued that the formulae provided have to be simplified in order to be used in practice. Since usual values of the relative reinforcement length ζ_r is about 80% and the parameter β is normally rather high (i.e. larger than 10), Eq. (26) can be simplified as follows:

$$f_{\tau\,\max}(\beta, \zeta_r) \cong 1 + \beta(1 - \zeta_r). \tag{51}$$

By substituting Eq. (51) into Eq. (25), we obtain an approximate value of the maximum shearing stress, which is plotted in Fig. 4. As can be seen, for high ζ_r values, the correct and approximate values of τ_{max} are almost coincident.

According to Eq. (51), the critical load estimate (41) becomes:

$$P_c = \sqrt{\frac{1+4\rho}{\rho}}\sqrt{2t_r t_b h_b E_b G_c}\,\frac{h_b}{3l}\,\frac{\beta}{1+\beta\,(1-\zeta_r)}. \tag{52}$$

It can be easily proven that, for $\zeta_r > 0.6$ and $\beta > 6$, the relative error that occurs by using Eq. (52) instead of Eq. (41) is always less than 2%. Furthermore, Eq. (52) is conservative with respect to Eq. (41), since, in the same range, it provides always lower critical load predictions. Finally, observe that neglecting unity at the denominator of the last fraction at the right-hand side of Eq. (52) is equivalent to using the EB model, i.e. Eq. (6); in such a case, with respect to Eq. (41), the critical load may be overestimated by more than 100% for the same range of the parameters given above (see Fig. 9 and related discussion).

8. Conclusions

In the present paper we analysed the edge debonding failure mechanism for beams strengthened by FRP strips. Although this collapse mode has been widely studied in the last decade, the present analysis focused on two aspects that, in the authors' opinion, have not received the right attention up to now:

- The link between the stress analysis and the energy approach. A general rule to bypass the complex energetic analysis when the interface between the beam and the reinforcement is described by a spring model has been proven and applied to the three point bending geometry.
- The post-peak structural response. The load versus deflection diagrams have been obtained and analysed, highlighting the presence of crack instabilities, i.e. snap–back and snap-through phenomena. Finally, the size effect has been pointed out by means of a dimensional analysis.

In order to obtain analytical results, we considered only relatively simple models: in the authors' opinion they are the right compromise between simplicity and accuracy. More refined models can now be found in the literature (see e.g. [33]).

Although in the present paper we considered only a TPB geometry, the procedure outlined here can be applied to other geometries as well (e.g. the push–pull direct shear test). However, difficulties are expected with statically indeterminate geometries, for which the determination of the shearing stress within the adhesive layer may become notably more complicated (i.e. the right-hand sides in Eqs. (11) and (12) are a priori unknown).

For what concerns the approximations used in the developed model, it is worth observing that:

- For the push–pull direct shear test, it has been proven [31,32] that the maximum load causing the FRP debonding is independent of the shape of the cohesive law of the interface, whereas it depends only on the interfacial fracture energy (for a sufficiently large bonded length). Therefore, it is argued that taking into account, for instance, a cohesive law with linear softening (Fig. 7) instead of the linear-purely brittle law considered herein could affect only slightly the load triggering the FRP debonding mechanism.
- According to the analysis performed by Rabinovitch [9], the peeling stresses (as well as a 2D elastic modelling of the adhesive) seem to affect slightly the value of the strain energy release rate of a three point bending strengthened beam.

Finally, the formulae provided within the present theoretical approach have to be validated by comparison with experimental data on concrete as well as on metallic FRP strengthened beams and with numerical analyses such as [34].

Appendix A

The aim of the appendix is to show the equivalence between the local approach and the global approach for the computation of the SERR. The former has been exploited in the paper. The latter one is based on Eq. (30) and was applied numerically by Rabinovitch [9] by means of the Virtual Crack Extension Method.

However, although complicated, it is still possible to proceed analytically. In such a way it is possible to show that the two approaches provide exactly the same result.

To apply Eq. (30), the strain energy Φ of the composite structure has to be computed. It is the sum of four terms, i.e. the strain energy within the FRP strip (Φ_r), the adhesive layer (Φ_a), the portion of the beam above the FRP (Φ_{b1}) and where there is no reinforcement (Φ_{b2}). The first, the second and the fourth contributions are straightforward:

$$\Phi_r = \frac{h_r}{2E_r}\int_0^{z_r} \sigma_r^2 \, \mathrm{d}z \tag{A.1}$$

$$\Phi_a = \frac{h_a}{2G_a}\int_0^{z_r} \tau_a^2 \, \mathrm{d}z \tag{A.2}$$

$$\Phi_{b2} = \frac{1}{2}\int_{z_r}^{l} \frac{M^2}{E_b I_b} \, \mathrm{d}z. \tag{A.3}$$

About the third contribution (Φ_{b1}), it should be noted that, by marking with ε_{bG} the axial dilation of the centre of gravity of the cross section (without the reinforcement, i.e. $y = h/2$), classical beam theory yields:

$$\Phi_{b1} = \frac{E_b A_b}{2}\int_0^{z_r} \varepsilon_{bG}^2 \, \mathrm{d}z + \frac{E_b I_b}{2}\int_0^{z_r} \chi_b^2 \, \mathrm{d}z \tag{A.4}$$

where $A_b = t_b h_b$. The two integrand functions can be expressed as functions of ε_r by means of Eq. (14) and of the relationship $\varepsilon_{bG} = \rho\varepsilon_r$, which is derived from Eq. (11). Since $\sigma_r = E_r\varepsilon_r$, from Eqs. (A.3) and (A.4) we get:

$$\Phi_b = \Phi_{b1} + \Phi_{b2} = \frac{2E_b t_b h_b \rho^2}{E_r^2}\int_0^{z_r} \sigma_r^2 \, \mathrm{d}z - \frac{3P\rho}{E_r h_b}\int_0^{z_r} \sigma_r \, (l - z) \, \mathrm{d}z + \frac{P^2 l^3}{2E_b t_b h_b^3} \tag{A.5}$$

where the third term at the right-hand side represents the strain energy of the beam without reinforcement. By substitution of Eq. (22) into (A.1)–(A.5) and of Eq. (23) into (A.2) and skipping analytical details, we finally obtain:

$$\Phi = \frac{P^2 l^3}{2E_b t_b h_b^3}\left\{1 - \frac{9\rho}{1+4\rho}\int_0^{\zeta_r}\left[2\,(1-\zeta)\,f_\sigma(\beta,\zeta,\zeta_r) - f_\sigma^2(\beta,\zeta,\zeta_r) - \frac{f_\tau^2(\beta,\zeta,\zeta_r)}{\beta^2}\right]\mathrm{d}\zeta\right\}. \tag{A.6}$$

By means of Eqs. (20), (24) and (26), it is then possible to check the following equality:

$$\int_0^{\zeta_r}\left[2\,(1-\zeta)\,f_\sigma(\beta,\zeta,\zeta_r) - f_\sigma^2(\beta,\zeta,\zeta_r) - \frac{f_\tau^2(\beta,\zeta,\zeta_r)}{\beta^2}\right]\mathrm{d}\zeta = \int_0^{\zeta_r}\frac{f_{\tau max}^2(\beta,\zeta_r)}{\beta^2}\mathrm{d}\zeta_r. \tag{A.7}$$

Eq. (A.7) shows that Eq. (A.6) coincides with Eq. (45). This means that the derivative of Eq. (A.6) with respect to the crack surface, i.e. Eq. (30), provides the same analytical expression of the SERR given by Eq. (39), thus proving the equivalence between the global and the local strategies for the computation of the SERR. On the other hand, it is evident that, in the present case, the local approach is by far more effective.

Appendix B

The explicit expression of the integral at the right-hand side of Eq. (45) is:

$$\int_0^{\zeta_r}\frac{f_{\tau\max}^2(\beta,\zeta_r)}{\beta^2}\mathrm{d}\zeta_r = \zeta_r\left(1 - \zeta_r + \frac{\zeta_r^2}{3}\right) - \frac{\beta\zeta_r + 2\beta\,(1-\zeta_r)\,[1-\mathrm{sech}(\beta\zeta_r)] + [\beta^2\,(1-\zeta_r)^2 - 1]\tanh(\beta\zeta_r)}{\beta^3}. \tag{B.1}$$

Its substitution into Eqs. (45) and (47) provides the analytical expressions of the strain energy and of the deflection. The first addend corresponds the equivalent beam model whereas the second one represents the correction of the shear lag model, which vanishes as $\beta \to \infty$. On the other hand, because of Eq. (40b), the integral (B.1) is zero if $\beta \to 0$.

References

[1] Hollaway L, Leeming M. Strengthening of reinforced concrete structures. Cambridge (England): Woodhead Publishing; 1999.
[2] Zerbo V, Di Tommaso A, Ceriolo L. FRP strengthening systems for metallic structures: A state of the art. In: Proceedings of structural analysis of historical constructions. London (England): Balkema; 2004.
[3] Fib Task Group 9.3. Externally bonded FRP reinforcement for RC structures, fib CEB-FIP Bulletin 14. Switzerland; 2001.
[4] ACI Committee 440. ACI 440.2R-02 guide for the design and construction of externally bonded FRP systems for strengthening concrete structures. USA; 2002.
[5] CNR. CNR-DT 200/2004. Istruzioni per la progettazione, l'esecuzione ed il controllo di interventi di consolidamento statico mediante l'utilizzo di compositi fibrorinforzati. Italy; 2004.
[6] Cornetti P, Puzzi S, Carpinteri A. Failure mechanisms in beams strengthened with adhesive strips. In: Proceedings of the XVIII national conference of theoretical and applied mechanics. 2007.
[7] Carpinteri A, Cornetti P, Pugno N. Debonding of FRP strengthened beams: Stress assessment versus fracture mechanics approach. In: Carpinteri A, Gambarova P, Ferro G, Plizzari G, editors. Proceedings of the 6th international FraMCoS conference, vol. 2. London: Taylor & Francis; 2007. p. 1053–60.
[8] Muckopadhyaya P, Swamy N. Interface shear stress: A new design criterion for plate debonding. J Composite Construct 2001;5:35–43.
[9] Rabinovitch O. Fracture-mechanics failure criteria for RC beams strengthened with FRP strips—A simplified approach. Compos Struct 2004;64:479–92.
[10] Colombi P. Reinforcement delamination of metallic beams strengthened by FRP strips: Fracture mechanics based approach. Eng Fract Mech 2006;73:1980–95.
[11] Volkersen O. Rivet strength distribution in tensile-stressed rivet joints with constant cross-section. Luftfahrforschung 1938;15:41–7.
[12] Vilnay O. The analysis of reinforced concrete beams strengthened by epoxy bonded steel plates. Int J Cement Composite Lightweight Concr 1988;10:73–8.
[13] Triantafillou TC, Deskovic N. Innovative prestressing with FRP sheets: Mechanics of short-term behaviour. J Eng Mech 1991;117:1652–72.
[14] Taljsten B. Strengthening of beams by plate bonding. ASCE J Mater Civil Eng 1997;9:206–12.
[15] Malek A, Saadatmanesh H, Ehsani M. Prediction of failure load of R/C beams strengthened with FRP plate due to stress concentration at the plate end. ACI Struct J 1998;95:142–52.
[16] Smith S, Teng J. Interfacial stresses in plated beams. Eng Struct 2001;23:857–71.
[17] Carpinteri A. Interpretation of the Griffith instability as a bifurcation of the global equilibrium. In: Shah S, editor. Application of fracture mechanics to cementitious composites. Dordrecht: Martinus Nijhoff Publishers; 1985. p. 287–316.
[18] Carpinteri A. Cusp catastrophe interpretation of fracture instability. J Mech Phys Solids 1989;37:567–82.
[19] Carpinteri A. Decrease of apparent tensile and bending strength with specimen size: Two different explanations based on fracture mechanics. Internat J Solids Structures 1989;25:407–29.
[20] Biolzi L, Cangiano S, Tognon G, Carpinteri A. Snap–back softening instability in high strength concrete beams. Mater Struct (RILEM) 1989;22:429–36.
[21] Andrews MG, Massabò R, Cox BN. Elastic interaction of multiple delaminations in plates subject to cylindrical bending. Internat J Solids Structures 2006;43:855–86.
[22] Greco F, Lonetti P, Nevone Blasi P. An analytical investigation of debonding problems in beams strengthened using composite plates. Eng Fract Mech 2007;74:346–72.
[23] Carpinteri A, Lacidogna G, Paggi M. On the competition between delamination and shear failure in retrofitted concrete beams and related scale effects. In: Carpinteri A, Gambarova P, Ferro G, Plizzari G, editors. Proceedings of the 6th international FraMCoS conference, vol. 2. London: Taylor & Francis; 2007. p. 1069–76.
[24] Ferracuti B, Savoia M, Mazzotti C. A numerical model for FRP-concrete delamination. Composites: Part B 2006;37:356–64.
[25] Stang H, Li Z, Shah SP. Pullout problem: Stress versus fracture mechanical approach. J Eng Mech 1990;116:2136–50.
[26] Pugno N, Carpinteri A. Tubular adhesive joints under axial load. J Appl Mech 2003;70:832–9.

[27] Yuan H, Teng JG, Seracino R, Wu ZS, Yao J. Full-range behavior of FRP-to-concrete bonded joints. Eng Struct 2004;26:553–65.
[28] Leung CKY, Yang Y. Energy-based modeling approach for debonding of FRP plate from concrete substrate. ASCE J Eng Mech 2006;132:583–93.
[29] Cavallera D. Reinforcement delamination of metallic beams strengthened by FRP strips: A fracture mechanics approach. MS thesis. Torino (Italy); 2007.
[30] Carpinteri A. Development of realistic concrete models including scaling effects. Final report to the commission of the European communities, reactor safety programme 1985–87. Ispra (Italy); 1989.
[31] Wu Z, Yuan H, Niu H. Stress transfer and fracture propagation in different kinds of adhesive joints. J Eng Mech ASCE 2002;128:562–73.
[32] Ferracuti B, Savoia M, Mazzotti C. Interface law for FRP–concrete delamination. Compos Struct 2007;80:523–31.
[33] Rabinovitch O. Stress cohesive interface modeling of debonding failure in FRP strengthened beams. J Eng Mech ASCE 2008;134:578–88.
[34] Carpinteri A, Lacidogna G, Paggi M. Acoustic emission monitoring and numerical modeling of FRP delamination in RC beams with non-rectangular cross-section. Mater Struct 2007;40:553–66.